12th International Symposium on Turbulence and Shear Flow Phenomena (TSFP12)
Osaka, Japan (Online), July 19-22, 2022

ROUGHNESS FUNCTION AND TURBULENT STATISTICS WITH INCREASING ROUGHNESS SIZE FROM DIRECT NUMERICAL SIMULATIONS

Hiten Mulchandani
Department of Engineering
University of Cambridge
Trumpington Street, Cambridge CB2 1PZ
hm650@cam.ac.uk

Ricardo Garcia-Mayoral
Department of Engineering
University of Cambridge
Trumpington Street, Cambridge CB2 1PZ
r.gmayoral@eng.cam.ac.uk

ABSTRACT

We present results of fully resolved, direct numerical simulations (DNSs) of turbulent flows over regular arrays of cylindrical roughness elements. DNSs were conducted for $k^+ = 5, 10, 15$, and 20 at $Re_\tau \approx 190$ and for $k^+ = 20, 40$, and 60 at $Re_\tau \approx 380$, ranging from the onset of the transitionally rough regime through to the fully rough regime. Data from the DNSs are presented and discussed for the roughness function, equivalent sand-gain roughness, mean flow velocity profiles, turbulence statistics, and spectral energy densities. Results suggest there is a progressive departure from smooth-wall-like turbulence for all cases except the smallest roughness size investigated. We hypothesise the differences are related to the nonlinear interaction of the texture-coherent flow with the background turbulence and plan to assess the importance of this mechanism in future work.

Introduction

Many engineering surfaces are rough and cause additional drag compared to smooth surfaces, and it is of industrial interest to quantify this drag. Sufficiently far above the roughness elements, it is commonly accepted that smooth- and rough-wall turbulence behave in a similar manner in what is known as outer-layer similarity (Clauser, 1956; Townsend, 1956). The effect of the roughness reduces, then, to an offset in the mean velocity profile of a rough wall relative to that of a smooth wall in the log layer. This is given by the roughness function, $\Delta U^+ = U_S^+ - U_R^+$, measured in the log layer, where the superscript '+' indicates wall-unit scaling with kinematic viscosity and the friction velocity, and the subscripts 'S' and 'R' indicate smooth and rough walls, respectively. Defining the skin-friction coefficient as $C_f = \tau_w/(\rho U_\delta^2/2) = 2/U_\delta^{+2}$, the impact of ΔU^+ on C_f through the decrease in U_δ^+ for rough walls becomes immediately apparent (Spalart & McLean, 2011; García-Mayoral & Jiménez, 2011; García-Mayoral *et al.*, 2019; Chung *et al.*, 2021). When expressed in wall units, ΔU^+ is generally believed to be independent of the Reynolds number for a given roughness geometry and size, k^+ (Flack *et al.*, 2007). In turn, the change in C_f depends on the Reynolds number through the reference smooth U_δ^+. The offset increases with k^+, but how it varies greatly depends on the roughness geometry and is difficult to predict *a priori* (Jiménez, 2004; Chung *et al.*, 2021). To circumvent this difficulty, an equivalent "sand-grain roughness", k_s^+, is often employed to characterize the effect of the surface, so that the actual surface is referred to the sand-grain surface that produced the same ΔU^+ in the pioneering experiments of Nikuradse (1933). This, however, simply transfers the problem from predicting ΔU^+ to predicting k_s^+, as there is a one-to-one relationship between both quantities (Bradshaw, 2000; Abderrahaman-Elena *et al.*, 2019). Furthermore, the ratio k_s/k for a given surface only becomes constant in the fully rough regime (Jiménez, 2004; Chung *et al.*, 2021), when it becomes equal to $k_{s,\infty}^+/k^+$ and the curve $k_{s,\infty}^+$-ΔU^+ becomes universal. This implies that k_s^+, like ΔU^+, does not exclusively depend on the surface geometry but also on the flow, i.e., it is a hydraulic property, and only becomes a geometric property in the fully rough regime. It is therefore important to understand the physical mechanisms at play in determining ΔU^+, or k_s^+, up to the roughness size for which the flow becomes fully rough. Beyond this point, once the curve becomes universal, the practical interest in understanding the physical mechanisms is more limited.

Toward this aim, we conduct fully resolved, direct numerical simulations (DNSs) of turbulent flows over regular arrays of cylindrical roughness elements. The roughness function varies from the onset of the transitionally rough regime through to the fully rough regime. When the roughness is much smaller than the smallest eddies in the near-wall flow, $k^+ << 20$, the overlying turbulent flow perceives the near-wall flow to be smooth-wall-like (Abderrahaman-Elena *et al.*, 2019; Ibrahim *et al.*, 2021) and the roughness is perceived as a homogenised boundary condition by the overlying flow (Bottaro, 2019). As the roughness size becomes comparable to the size of the near-wall turbulent eddies, the overlying flow begins to

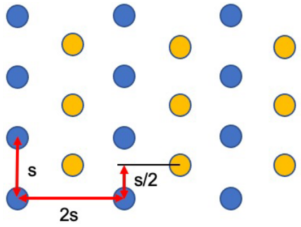

Figure 1. Schematic plan view of the staggered cylindrical roughness elements investigated, from Vishwanathan *et al.* (2021).

perceive the non-homogeneity of the texture. In the context of alternating slip/no-slip textures, Fairhall *et al.* (2019) observed that the overlying flow still perceived a homogenised boundary condition from the surface up to $k^+ \approx 50$, but noted that the texture caused additional dissipation in the flow above from $k^+ \approx 15$. Fairhall *et al.* (2019) proposed that this additional dissipation was caused by the nonlinear interaction between the texture-coherent flow and the background, texture-incoherent turbulence. We aim to assess the importance of this mechanism for roughness, and ultimately to aid in the development of physics-based models that can predict ΔU^+ *a priori* without resorting to costly experiments, simulations, or correlations (if available) to similar surfaces.

Numerical Method

The DNSs solve the incompressible flow in a periodic channel driven by a constant mean pressure gradient with roughness on the top and bottom walls, imposed using immersed boundaries, using a code adapted from Sharma & García-Mayoral (2020*a*,*b*). The channel is of size $2\pi\delta$ x $2(\delta + k)$ x $\pi\delta$ in the streamwise, wall-normal, and spanwise directions, respectively, where δ is the channel half-height from the tips of the roughness to the center of the channel and k is the roughness height. A spectral discretisation is employed in the streamwise and spanwise directions and a second-order central difference scheme on a staggered grid is employed in the wall-normal direction. The grid is stretched such that $\Delta y^+_{min} \approx 0.4$ near the walls and $\Delta y^+_{max} \approx 4$ in the center. The code uses a 'multiblock' grid which allows finer resolution near the walls compared to the channel center to properly resolve the flow between the roughness elements. At the center of the channel, the grid resolution is standard for DNSs, with $\Delta x^+ \leq 8$ and $\Delta z^+ \leq 4$. The resolution near the walls in the streamwise and spanwise directions is given in Table 1 for the list of the cases investigated at their respective frictional Reynolds numbers. Time integration is carried out using a three-step Runge–Kutta scheme with a fractional step, pressure correction method that enforces continuity (Le & Moin, 1991), for which the time-step is set by a fixed advective CFL number of 0.7.

A schematic illustration of the staggered pattern of cylindrical roughness elements used in the simulations is shown in Figure 1. The ratio of element spacing to its height was fixed at $s/k = 3.46$ and the ratio of element diameter to its spacing was fixed at $d/s = 0.45$. The instantaneous flow realizations in Figure 2 show simulation results over the texture geometry for $k^+ = 10, 15$, and 20 at $Re_\tau \approx 190$.

Table 1. Roughness height, frictional Reynolds number, and resolution near the walls in the streamwise and spanwise directions for the cases investigated. Simulations marked with the $(^*)$ superscript are from Adams (2021).

Name	k^+	Re_τ	Δx^+	Δz^+
K05*	5.25	187	0.96	0.96
K10*	10.36	188	1.44	1.44
K15*	15.61	190	2.16	2.16
K20a*	20.89	191	2.89	2.89
K20b*	20.73	379	2.89	2.89
K40	42.51	389	2.89	2.89
K60	64.67	399	2.89	2.89

Results and Analysis

The measured roughness function against equivalent sand-grain roughness is shown in Figure 3 for the cases studied, overlaid with values for other rough surfaces from Jiménez (2004). The cases investigated range from the onset of the transitionally rough regime, for $k^+ \approx 5$, through to the fully rough regime beyond $k^+ = 15$. The roughness function measured from the DNSs, ΔU^+_m, is obtained by subtracting the rough-wall mean velocity profile from the smooth-wall mean velocity profile and averaging over the log layer.

Figure 4 presents a comparison between the measured roughness function from the DNSs and the corresponding predicted values. The predicted roughness function, ΔU^+_p, is obtained as follows. We define $y^+ = 0$ at the plane of the roughness tips. For small roughness, $k^+ \approx 5$, turbulence is smooth-wall-like, except for an offset, ℓ^+_T, such that it perceives an apparent 'virtual' origin at $y^+ = -\ell^+_T$ (Luchini, 1996; Ibrahim *et al.*, 2021). Turbulence then remains essentially unchanged compared to that over a smooth wall, except for an offset given by the virtual origin. We find the value of the offset by fitting the curve representing the Reynolds shear stress to smooth-wall data, as shown in Figure 5(*f*). As long as turbulence remains smooth-wall-like, the smooth-wall and rough-wall Reynolds stresses collapse. From a mean momentum balance, this implies that the mean velocity profiles for rough and smooth walls will curve in the same way above the tips, but will be offset by a constant value which can, for instance, be measured at the plane of the tips (Gómez-de Segura & García-Mayoral, 2019). At this plane, the mean velocity for the rough case is U^+_t, while at the corresponding plane the smooth-wall mean velocity is $U^+_S(y^+ = \ell^+_T)$. The predicted roughness function assuming smooth-wall-like turbulence is thus $\Delta U^+ = U^+_S(y^+ = \ell^+_T) - U^+_t$, as portrayed in Figure 4. Discrepancies in the results between the measured and predicted ΔU^+ for $k^+ > 5$ suggest that a virtual origin framework is insufficient to accurately estimate the roughness function beyond the smallest roughness size.

Mean velocity profiles, turbulent velocity fluctuations, and Reynolds stresses are shown in Figure 5 for $k^+ = 5$ to $k^+ = 20$ at $Re_\tau \approx 190$. For small roughness, $k^+ = 5$, there is good collapse of the mean streamwise velocity and the wall-normal and spanwise root mean square (r.m.s.) velocity fluctuations shifted by the virtual origin onto the smooth-wall profile. The streamwise r.m.s. velocity fluctuations, however,

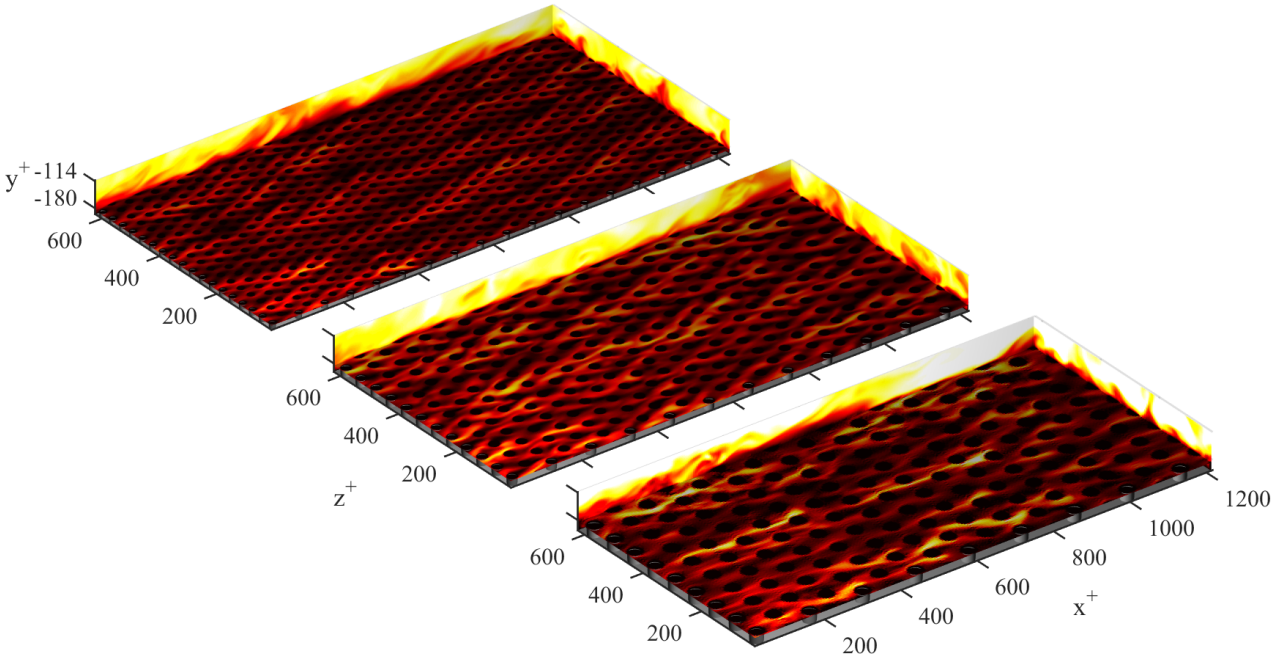

Figure 2. Instantaneous realizations of the fluctuating streamwise velocity from the DNSs of a regular array of cylindrical roughness elements at $k^+ = 10, 15$, and 20 at $Re_\tau \approx 190$.

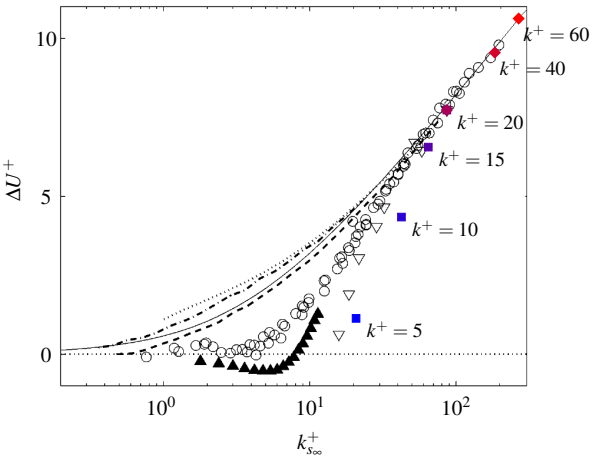

Figure 3. Roughness function against equivalent sand-grain roughness for the present regular staggered cylinders (squares for $Re_\tau \approx 190$ and diamonds for $Re_\tau \approx 380$), compared with uniform sand (circles), uniform packed spheres (white triangles), galvanised iron (dotted line), tar-coated cast iron (dashed line), wrought iron (dotted dashed line), interpolation (solid line) and riblets (black triangles). Adapted from Jiménez (2004).

do not collapse onto the smooth-wall profile near the wall. Ibrahim *et al.* (2021) argued that this does not essentially affect the structure of near-wall turbulence, as the latter's virtual origin is essentially determined by the origin perceived by the quasi-streamwise vortices, which mainly induce only wall-normal and spanwise velocities near the surface. For larger roughness sizes, the near-wall cycle is more severely disrupted and turbulence is no longer smooth-wall-like, as evidenced by a lack of collapse of the data for $k^+ \geq 10$.

Previous studies suggest that for roughness sizes $k^+ \leq 20$, it is sufficient to conduct simulations at $Re_\tau \approx 200$ to capture the effect on the outer layers of the flow, i.e., the roughness function (Abderrahaman-Elena *et al.*, 2019). To analyze the effect of frictional Reynolds number on the mean velocity profile and turbulence statistics, we compare the results at $Re_\tau \approx 187$ with $Re_\tau \approx 376$ for $k^+ = 20$, in contrast with the results at $Re_\tau \approx 180$ with $Re_\tau \approx 360$ for smooth-wall data, as shown in Figure 6. For smooth-wall data, the observed differences are consistent with changes observed in the frictional Reynolds number. For rough-wall data, the trends in the mean velocity profiles are very similar at the two frictional Reynolds numbers. Away from the roughness elements, $y^+ > 50$, the Reynolds stresses from rough-wall simulations coincide with those from smooth-wall simulations at their corresponding frictional Reynolds numbers, which is indicative of the recovery of outer-layer similarity. Minor differences in the collapse are caused by small differences in the corresponding frictional Reynolds numbers. These arguments support the use of DNSs at a low frictional Reynolds number.

From the observations of Fairhall *et al.* (2019) in the context of the alternating slip/no-slip textures mentioned earlier, the differences that arise from extra Reynolds stresses are hypothesised to be due to the nonlinear interaction of the background turbulence with the dispersive flow. The spectral energy densities in Figure 7, which portray the distribution of energy across different length scales in the flow at $y^+ = 4$ above the roughness tips, demonstrate these effects. There is a progressive departure from smooth-wall energy densities towards shorter and wider wavelengths as the roughness height increases from $k^+ = 5$ to $k^+ = 60$. The nonlinear interaction between the texture-coherent flow and background turbulence is evident from the distortion in energy contours in the vicinity of the concentration of energy representing the texture-induced flow from $k^+ = 10$ onward. We are interested in characterizing deviations from smooth-wall turbulence and the dispersive flow from this data.

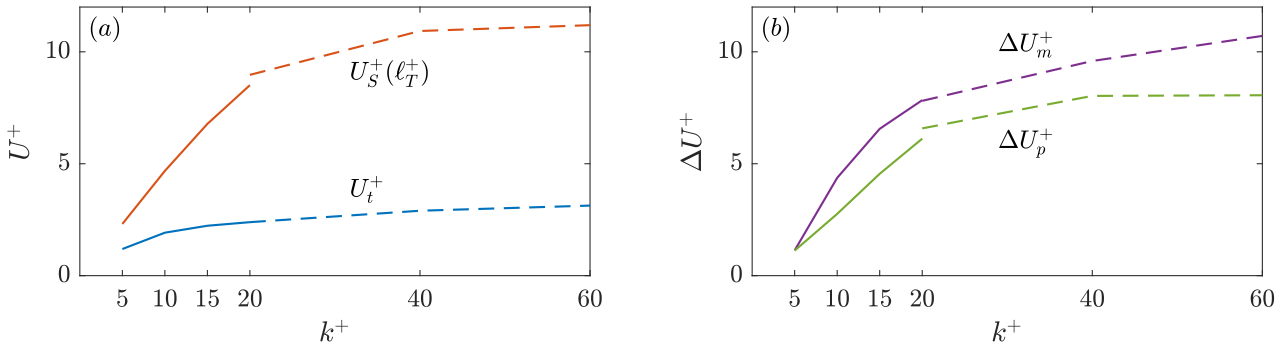

Figure 4. Results for (a) the mean velocity at $y^+ = 0$ for the rough walls, U_t^+, at $Re_\tau \approx 190$ (——) and $Re_\tau \approx 380$ (- - - -) and a smooth wall, $U_S^+(\ell_T^+)$, at $Re_\tau \approx 190$ (——) and $Re_\tau \approx 380$ (- - - -), and (b) measured values of the roughness function from the DNSs, ΔU_m^+, at $Re_\tau \approx 190$ (——) and $Re_\tau \approx 380$ (- - - -) and corresponding predicted values from the virtual origin framework, ΔU_p^+, at $Re_\tau \approx 190$ (——) and $Re_\tau \approx 380$ (- - - -).

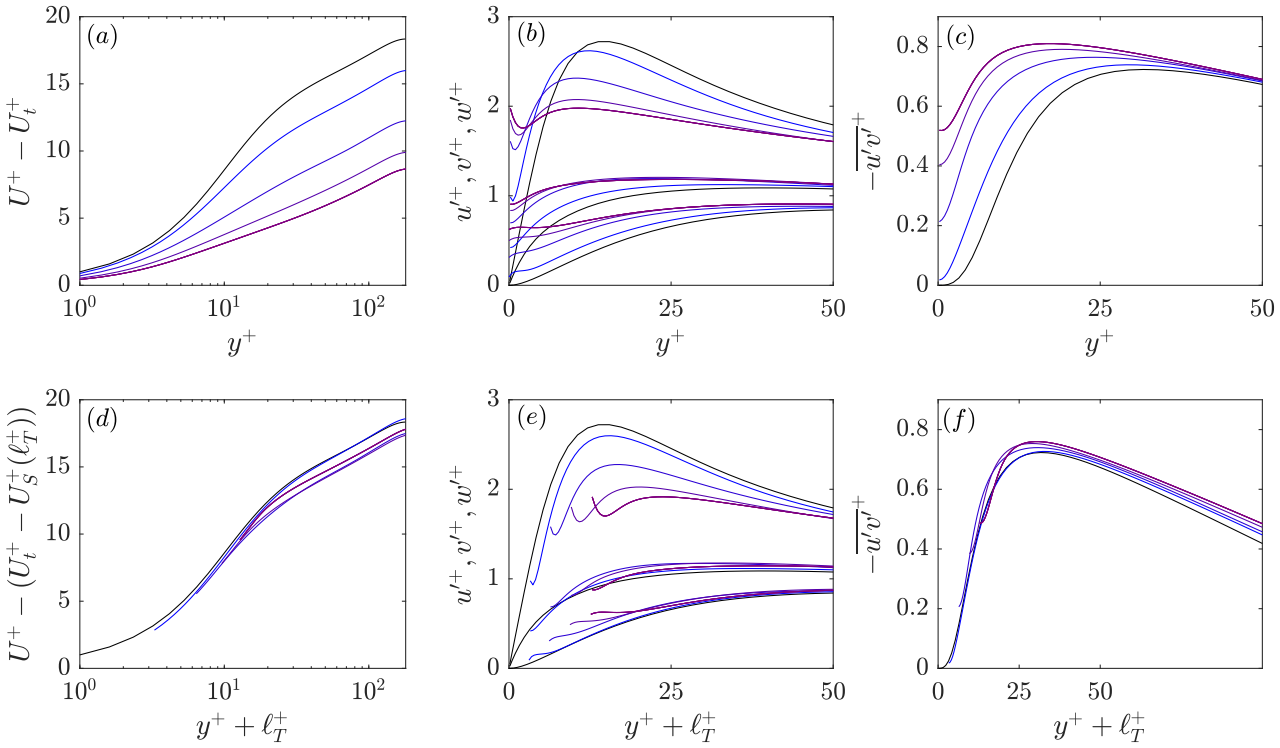

Figure 5. Results from DNSs for $k^+ \approx 5$ (——), $k^+ \approx 10$ (——), $k^+ \approx 15$ (——), and $k^+ \approx 20$ (——) with $Re_\tau \approx 190$, and a smooth wall with $Re_\tau \approx 180$ (——) for (a) the mean streamwise velocity profile with the velocity at the tips subtracted, (b) r.m.s. velocity fluctuations, (c) Reynolds shear stresses, (d) mean streamwise velocity profile shifted by the turbulent virtual origin with the predicted velocity at the virtual origin subtracted, (e) r.m.s. velocity fluctuations shifted by the virtual origin, and (f) Reynolds stresses shifted by the virtual origin.

Acknowledgments

This work has been partially supported by EPSRC-UK under grant EP/S013083/1. H.M. is supported by the Cambridge Commonwealth, European and International Trust. Computational resources were provided by the Cambridge Service for Data Driven Discovery under EPSRC-UK Tier-2 grant EP/P020259/1 and by the ARCHER2 system under PRACE grant pr1u1702-ESTONT.

Summary

In this paper, results from DNSs of turbulent flows over regular arrays of cylindrical roughness elements are presented and discussed. DNSs were conducted for $k^+ = 5, 10, 15$, and 20 at $Re_\tau \approx 190$ and for $k^+ = 20, 40$, and 60 at $Re_\tau \approx 380$, ranging from the onset of the transitionally rough regime through to the fully rough regime. Mean streamwise velocity profiles, turbulence statistics, and spectral energy densities from the DNSs suggest there is a progressive departure from

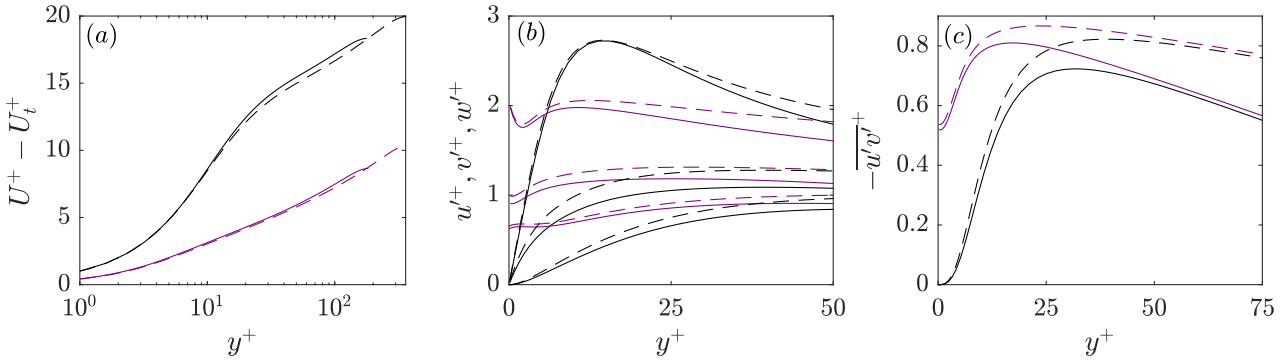

Figure 6. Results from the DNSs for $k^+ \approx 20$ at $Re_\tau \approx 187$ (———) and $Re_\tau \approx 376$ (- - - -), and a smooth wall at $Re_\tau \approx 180$ (———) and $Re_\tau \approx 360$ (- - - -) for (a) the mean streamwise velocity profile with the velocity at the tips subtracted, (b) r.m.s. velocity fluctuations, and (c) Reynolds shear stresses.

smooth-wall-like turbulence for all cases except the smallest roughness size investigated. We hypothesise the differences are related to the nonlinear interaction of the texture-coherent flow with the background turbulence and plan to assess the importance of this mechanism in future work.

REFERENCES

Abderrahaman-Elena, Nabil, Fairhall, Chris T. & García-Mayoral, Ricardo 2019 Modulation of near-wall turbulence in the transitionally rough regime. *J. Fluid Mech.* **865**, 1042–1071.

Adams, Melissa 2021 Turbulent flows over cylindrical roughness. Master's thesis, University of Cambridge.

Bottaro, A. 2019 Flow over natural or engineered surfaces: an adjoint homogenization perspective. *J. Fluid Mech.* **877**, P1.

Bradshaw, P. 2000 A note on "critical roughness height" and "transitional roughness.". *Phys. Fluids* **12**, 1611–14.

Chung, Daniel, Hutchins, Nicholas, Schultz, Michael P. & Flack, Karen A. 2021 Predicting the drag of rough surfaces. *Annual Review of Fluid Mechanics* **53** (1), 439–471.

Clauser, F. H. 1956 The turbulent boundary layer. *Adv. Appl. Mech.* **4**, 1–51.

Fairhall, C. T., Abderrahaman-Elena, N. & García-Mayoral, R. 2019 The effect of slip and surface texture on turbulence over superhydrophobic surfaces. *J. Fluid Mech.* **861**, 88–118.

Flack, K. A., Schultz, M. P. & Connelly, J. S. 2007 Examination of a critical roughness height for outer layer similarity. *Physics of Fluids* **19** (9), 095104.

García-Mayoral, R. & Jiménez, J. 2011 Hydrodynamic stability and breakdown of the viscous regime over riblets. *J. Fluid Mech.* **678**, 317–347.

García-Mayoral, R, de Segura, G. Gómez & Fairhall, C. T. 2019 The control of near-wall turbulence through surface texturing. *Fluid Dynamics Research* **51** (1), 011410.

Ibrahim, Joseph I., Gómez-de Segura, Garazi, Chung, Daniel & García-Mayoral, Ricardo 2021 The smooth-wall-like behaviour of turbulence over drag-altering surfaces: a unifying virtual-origin framework. *J. Fluid Mech.* **915**, A56.

Jiménez, J. 2004 Turbulent flows over rough walls. *Annu. Rev. Fluid Mech* **36**, 173–196.

Le, H. & Moin, P. 1991 An improvement of fractional step methods for the incompressible Navier-Stokes equations. *J. Comput. Phys.* **92** (2), 369–379.

Luchini, P. 1996 Reducing the turbulent skin friction. In *Computational Methods in Applied Sciences '96*, pp. 466–470. John Wiley & Sons Ltd.

Nikuradse, J. 1933 Strömungsgesetze in rauhen rohren. *VDI-Forschungsheft* **361**.

Gómez-de Segura, G. & García-Mayoral, R. 2019 Turbulent drag reduction by anisotropic permeable substrates – analysis and direct numerical simulations. *J. Fluid Mech.* **875**, 124–172.

Sharma, A. & García-Mayoral, R. 2020*a* Scaling and dynamics of turbulence over sparse canopies. *J. Fluid Mech.* **888**, A1.

Sharma, A. & García-Mayoral, R. 2020*b* Turbulent flows over dense filament canopies. *J. Fluid Mech.* **888**, A2.

Spalart, Philippe R. & McLean, J. Douglas 2011 Drag reduction: enticing turbulence, and then an industry. *Phil. Trans. R. Soc.* **369**, 1556–1569.

Townsend, A. A. 1956 *The Structure of Turbulent Shear Flow*. Cambridge University Press.

Vishwanathan, Vidya, Fritsch, Danny, Lowe, Todd K & Devenport, William J 2021 Analysis of coherent structures over a smooth wall turbulent boundary layer in pressure gradient using spectral proper orthogonal decomposition. In *AIAA Aviation 2021 Forum*, p. 2893.

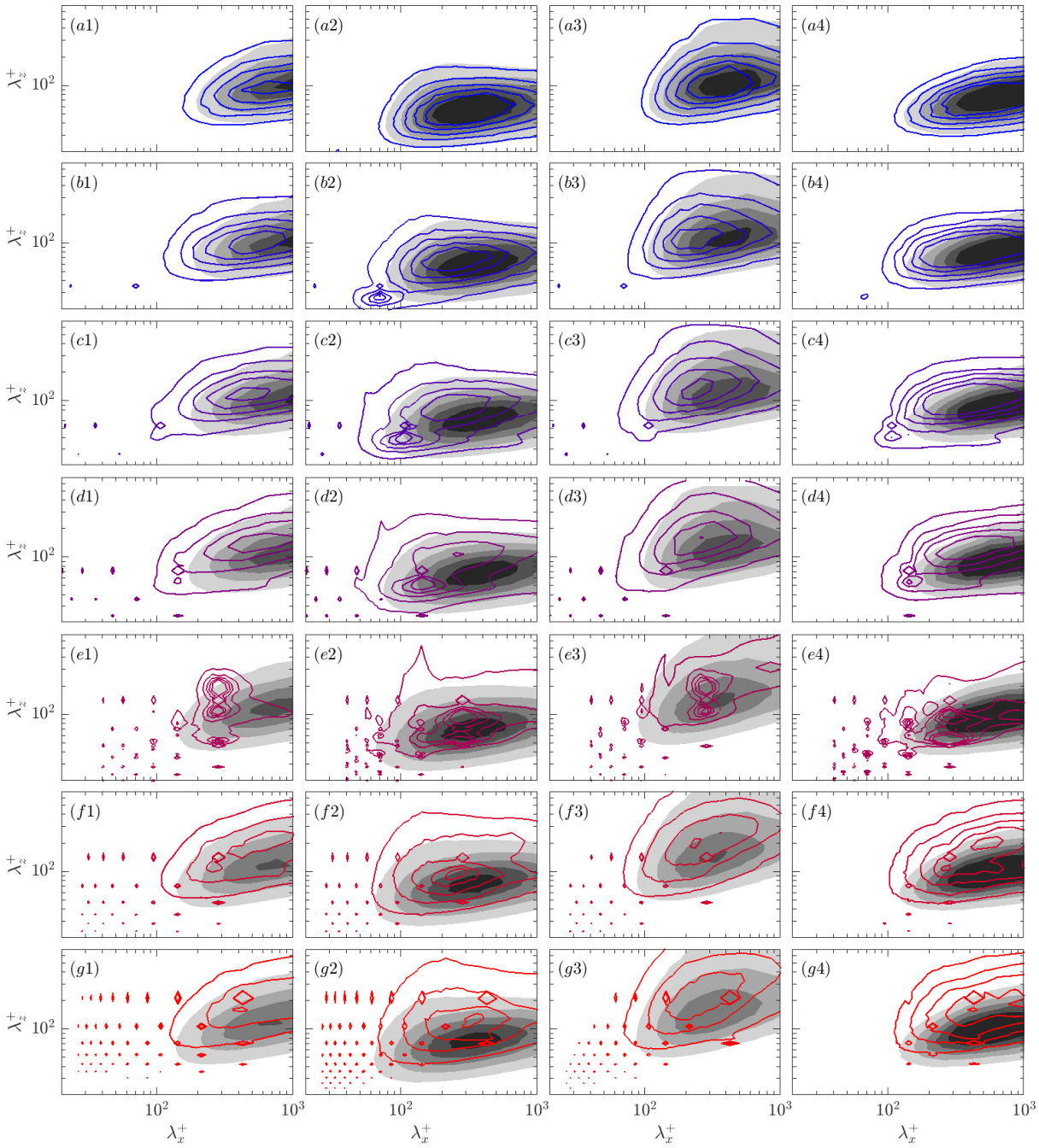

Figure 7. Pre-multiplied two-dimensional spectral energy densities at $y^+ \approx 4$ above the roughness tips for $(a1)-(g1)$ $k_x k_z E_{uu}^+$, $(a2)-(g2)$ $k_x k_z E_{vv}^+$, $(a3)-(g3)$ $k_x k_z E_{ww}^+$, and $(a4)-(g4)$ $-k_x k_z E_{uv}^+$. Results for $k^+ \approx 5$ (———), $k^+ \approx 10$ (———), $k^+ \approx 15$ (———), and $k^+ \approx 20$ (———) at $Re_\tau \approx 190$, $k^+ \approx 20$ (———), $k^+ \approx 40$ (———), $k^+ \approx 60$ (———) at $Re_\tau \approx 380$, and a smooth wall at $Re_\tau \approx 180$ and $Re_\tau \approx 360$ (filled contours).